Published in final edited form as:
Neurobiol Aging. 2012 May ; 33(5): 878–885. doi:10.1016/j.neurobiolaging.2010.08.007.

Antemortem amyloid imaging and β-amyloid pathology in a case with dementia with Lewy Bodies

Kejal Kantarci[1], **Chunhui Yang**[2], **Julie A. Schneider**[2,3], **Matthew L. Senjem**[1], **Denise A. Reyes**[1], **Val J. Lowe**[1], **Lisa L. Barnes**[3], **Neelum T. Aggarwal**[3], **David A. Bennett**[3], **Glenn E. Smith**[4], **Ronald C. Petersen**[5], **Clifford R. Jack Jr.**[1], and **Bradley F. Boeve**[5]

[1] Department of Radiology, Mayo Clinic, Rochester, Minnesota

[2] Rush Alzheimer's Disease Center, Rush University, Chicago, Illinois

[3] Department of Neurology, Rush University, Chicago, Illinois

[4] Departments of Psychiatry and Psychology, Mayo Clinic, Rochester, Minnesota

[5] Department of Neurology, Mayo Clinic, Rochester, Minnesota

Abstract

The association between antemortem [^{11}C]-Pittsburgh Compound B (PiB) retention and β-amyloid (Aβ) load, Lewy body (LB) and neurofibrillary tangle (NFT) densities were investigated in a pathologically confirmed case of dementia with LB (DLB). 76-year-old man presenting with a clinical diagnosis of DLB had undergone PiB–positron emission tomography (PET), ^{18}F FDG-PET and MRI 18 months before death. The pathologic diagnosis was DLB neocortical-type with low-likelihood of Alzheimer's disease by NIA-Reagan criteria. Sections from regions of interest (ROI) on post-mortem examination were studied. A significant correlation was found between cortical Aβ density and PiB retention in the 17 corresponding ROIs ($r=0.899$; $p<0.0001$). Bielschowsky silver stain revealed mostly sparse neocortical neuritic plaques; whereas diffuse plaques were frequent. There was no correlation between LB density and PiB retention ($r=0.13$; $p=0.66$); nor between NFT density and PiB retention ($r=-0.36$; $p=0.17$). The ROI-based analysis of imaging and histopathological data confirms that PiB uptake on PET is a specific marker for Aβ density, but cannot differentiate neuritic from diffuse amyloid plaques in this case with DLB.

Keywords

Dementia with Lewy bodies; amyloid imaging; PET; pathology; amyloid

Corresponding Author: Kejal Kantarci, MD Mayo Clinic 200 First Street SW Rochester, MN 55905 **Phone:** 507- 284 8548, **Fax:** 507-284 2405, kantarci.kejal@mayo.edu.

2. 1. 1 Disclosure Statements

The authors do not have any actual or potential conflicts of interests to disclose. This study was approved by the Mayo Clinic Institutional Review Board, and informed consent for participation was obtained from every subject and/or an appropriate surrogate.

1. Introduction

Lewy body (LB) disease is the second most common cause of neurodegenerative dementia after Alzheimer's disease (AD), and LB pathology is present in about 20-35% of cases with dementia [Galasko, et al.,1994, Hansen, et al.,1990, Joachim, et al.,1988, Schneider, et al., 2007, Zaccai, et al.,2005]. A majority of patients with dementia with Lewy bodies (DLB) are pathologically characterized by the presence of β-amyloid (Aβ) plaques along with α-synuclein LB deposits [McKeith, et al.,2005, Schneider, et al.,2007]. Antemortem diagnosis of Aβ deposition in DLB may play an important role in treatment decisions, as well as assessing responsiveness to treatments targeting disease specific pathologies [Thal, et al., 2006].

In vivo retention of the positron emission tomography (PET) tracer N-Methyl-[11C]2-(4′-methylaminophenyl)-6-hydroxybenzothiazole ([11C]PIB 6-OH-BTA-1), or the [^{11}C]-Pittsburgh Compound B (PiB) reflects the deposition of fibrillary Aβ in patients with AD [Bacskai, et al.,2007, Ikonomovic, et al.,2008]. Increased PiB binding is typically present in DLB in up to 80% of cases [Edison, et al.,2008, Maetzler, et al.,2009], however the specificity of *in vivo* PiB retention in DLB is less clear [Burack, et al.,2010, Fodero-Tavoletti, et al.,2007, Maetzler, et al.,2008]. Fluorescence microscopy demonstrated *in vitro* binding of PiB to the fibrillar, misfolded proteins in the substantia nigra LBs [Maetzler, et al.,2008]. In contrast, PiB binding was not observed in the Aβ plaque-free brain homogenates in DLB, and LBs did not significantly contribute to the PiB fluorescence stain in tissue sections [Fodero-Tavoletti, et al.,2007]. Furthermore, the regional pattern of antemortem PiB retention was in agreement with the distribution of Aβ pathology in three Parkinson disease with dementia patients at autopsy [Burack, et al.,2010]. To the best of our knowledge no study has yet directly correlated *in vivo* PiB retention in DLB with postmortem Aβ load and α-synuclein LB density using quantitative methods and region of interest (ROI) analysis.

Our objective was to determine the association between antemortem PiB retention and Aβ, LB, and neurofibrillary tangle (NFT) loads in a pathologically confirmed case of DLB.

2. Methods

2.1.Participant

This case participated in the Mayo Clinic Alzheimer's Disease Research Center and the Rush University Alzheimer's Disease Center programs. Participants in both centers undergo approximately annual clinical examinations, routine laboratory tests, neuropsychological tests, and ancillary neuroimaging studies.

2.2.Imaging Studies

All imaging studies were performed at the Mayo Clinic. Magnetic resonance imaging (MRI) examinations were performed at 3 Tesla including a 3D-MPRAGE acquisition for anatomical segmentation and labeling. PET images were acquired using a PET/CT scanner (DRX; GE Healthcare) operating in 3D mode. The patient was injected with 432MBq [^{11}C]PIB and 511MBq [^{18}F]fluorodeoxyglucose (FDG) on the same day with one hour between the PiB and the ^{18}F-FDG PET scan acquisitions Subjects were prepared for ^{18}F-FDG in a dimly lit room, with minimal auditory stimulation. A CT image was obtained for attenuation correction. After a 40-min (PiB) or 30-min (^{18}F-FDG) uptake period, the subjects were imaged. A 20-min PiB or an 8-min ^{18}F-FDG scan was obtained. The PiB PET acquisition consisted of four 5-min dynamic frames, acquired from 40 to 60 min after injection, and the ^{18}F-FDG image acquisition consisted of four 2-min dynamic frames,

acquired from 30 to 38 min after injection. Standard corrections were applied. The pixel size for PET images were 1.0 mm and the slice thickness was 3.3 mm. [Lowe, et al.,2009].

2.3. Pathological examination

Pathological examination was performed at the Rush Alzheimer Disease Center. The brain was removed 4 hours after death, and 1 cm slabs from the right hemisphere were fixed for 3 days in 4% paraformaldehyde. Tissue was dissected from the hippocampus, entorhinal cortex, anterior cingulate gyrus, midfrontal, middle temporal, inferior parietal cortex, basal ganglia, thalamus and midbrain; embedded in paraffin; and cut into 6 micron sections and stained with hematoxylin and eosin (H&E) and modified Bielschowsky silver stain [Mufson, et al.,1988], and antibodies to Aβ (1:600, 10D5, courtesy of Elan pharmaceuticals), PHF-tau (1:3000; AT8; Pierce Protein Research) and α-synuclein (LB509; 1:100; Invitrogen Corp). A board-certified neuropathologist with expertise in dementia reviewed all slides using standard diagnostic criteria [Braak and Braak,1991, McKeith, et al.,2005, McKhann, et al., 1984, Mirra, et al.,1991].

For the imaging–pathology co-localization, we chose 8 additional ROIs (total of 17) based on the known distribution of Aβ, LB and neurofibrillary tangle (NFT) pathologies in AD and DLB. We included regions that are known to have abundant Aβ (e.g. inferior precuneus), LB (e.g. amygdala) and NFT (e.g. hippocampus), and regions that are known to have lesser Aβ (e.g. hippocampus), LB (e.g. precentral gyrus) and NFT (e.g. calcarine cortex) in order to sample a wide spectrum of pathology.

All sections were mounted on electrostatically charged plus slides (Daigger and Co., Inc., Lincolnshire, IL), deparaffinized, dehydrated in alcohols and xylene and coverslipped with Permount. Immunostains were performed using the avidin-biotin-peroxidase method (ABC-Elite, Vector, Burlingame, CA) on an Automated Leica Bond immunostain (Leica Microsystems Inc., Bannockborn IL) with a pre-defined protocol [Bennett, et al.,2004, Schneider, et al.,2002]. Briefly, all sections are washed and blocked with normal serum; incubated with the primary antibody; washed and incubated with the biotinylated secondary antibody; and then the avidin-biotin-peroxidase complex (Vector laboratories). The chromagen for color development was 3,3′diaminobenzidine. Positive controls included neocortical tissue from known cases of AD (for amyloid and PHF immunostain) and Lewy body disease (α-synuclein immunostains).

The fractional area occupied by Aβ was determined using image analysis. An investigator blinded to imaging data outlined each ROI using Stereo Investigator 8.0 on a Microbrightfield Stereology System, instructed a grid to be randomly placed, and a motorized stage to stop at about 20% of the grid intersection points to obtain images for area analysis by the triangulation method using the NIH Image processing application (Image J 1.42g (http://rsbweb.nih.gov/ij/). All values for each region were averaged to obtain the mean fraction of Aβ. For modified Bielschowsky stained sections we counted neuritic plaques, diffuse plaques, and NFT in the area with the greatest density of each marker, using a graticule in one square mm area (× 100 magnification) in each region. Density (number/mm^2) of LB and PHF-tau NFT was determined through manual counts with the ROI area outlined by Stereo Investigator 8.0 as noted above, and 100% of the area counted.

2.4. PiB-PET quantitative analysis

PIB-PET quantitative image analysis was performed using the fully automated image processing pipeline which is described in detail [Jack, et al.,2008, Senjem, et al.,2005]. Briefly, the method includes gray matter (GM) sharpening of PET images using MRI and partial volume correction of CSF and tissue compartments using SPM5[Ashburner and

Friston, 2005]. PIB-PET cortical ratio images were calculated by dividing the each PiB-PET GM voxel value by the median value in the cerebellar GM region in the patient's MRI space. The global cortical PiB retention was calculated by taking the median value of the PIB-PET GM ratio from the bilateral parietal, posterior cingulate, precuneus, temporal, prefrontal, orbitofrontal, anterior cingulate GM regions in the anatomical labeling atlas [Jack, et al., 2008].

ROI-based pathology correlation was performed by reorienting the 3D MRI images to anatomically match to the photographed images of the 17 histological sections. ROIs that simulated the histological blocks were drawn on the matching MRI slice using the image analysis software Analyze 10.0 (Mayo Clinic). The median GM PiB retention ratio was calculated for each of the 17 ROIs from the PIB-PET GM ratio images and corrected for partial volume averaging of CSF in the MRI space (Figure 1). The entorhinal cortex and substantia nigra regions evaluated at autopsy were not analyzed because the sizes of the histological blocs were less than the resolution of PET in at least one dimension.

3. Results

The patient began exhibiting recurrent dream enactment behavior around age 50. The frequency and severity of the behaviors gradually increased over many years, but injuries rarely occurred. His cognitive decline became apparent at the age 66 and over the following year he developed obvious signs of parkinsonism, leading to a diagnosis of DLB. By age 72 recurrent visual hallucinations, fluctuations in cognition, visual illusions, and auditory hallucinations became apparent. A comprehensive evaluation at age 76 was notable for a Kokmen Short Test of Mental Status [Kokmen, et al.,1987] score of 28/38, hypokinetic dysarthria, and moderate symmetric parkinsonism. Polysomnography demonstrated increased electromyographic tone and flailing limb movements during REM sleep, thereby confirming the presence of REM sleep behavior disorder (RBD). He showed clear deficits in attention and processing speed (unable to complete Trail Making Test A or B, semantic fluency at the 2nd percentile), and visual construction (Rey-Osterreith Complex figure was severely distorted, <1st percentile), with far less impairment or normal performance on confrontation naming and delayed recall on verbal memory measures.

MRI showed mild atrophy of the hippocampi and mild periventricular white matter hyperintensities. Abnormal glucose metabolism was present in the temporoparietal cortices and prefrontal cortex on ^{18}F-FDG PET consistent with the typical pattern in AD. PiB retention was most significant in the frontal lobes where as the occipital lobes were relatively spared. The abundant PiB retention in the white matter was comparable to the non-specific PiB retention typically seen in the white matter, which was masked out of the cortical GM ROI analysis and global PiB retention ratio through partial volume correction of CSF and tissue compartments using the co-registered 3D- MRI [Jack, et al.,2008] (Figure 2). The global PiB retention ratio was 1.68, which would be classified as “PiB positive” according to the typically used cut-off of 1.50 [Jack, et al.,2008].

The patient underwent numerous pharmacologic manipulations with cholinesterase inhibitors, levodopa, dopamine agonists, memantine, psychostimulants, and atypical neuroleptics, but these never resulted in any obvious clinical benefits. He died at age 77.

At autopsy, the brain weighed 1020g, had moderate to severe cortical atrophy, mild to moderate hippocampal atrophy, moderate lateral ventricular enlargement, and pallor of the substantia nigra. H&E showed severe nigral degeneration but no other abnormalities. Bielschowsky silver stained showed NFT were moderate in the hippocampus and entorhinal cortices, and absent in neocortical regions; and neuritic plaques were sparse in the

midfrontal, middle temporal, and inferior parietal cortices corresponding to a Braak stage III neurofibrillary pathology and low likelihood of AD by NIA-Reagan criteria (Table). LB were found in the substantia nigra, entorhinal, anterior cingulate, midfrontal, middle temporal and inferior parietal cortices, consistent with a pathological diagnosis of DLB – neocortical type.

Aβ was more sensitive to plaques, compared to Bielshowsky silver stain (Table, Figure 3). Overall, the density of Aβ was greatest in the frontal lobes and lowest in the hippocampus (Table). Amyloid angiopathy was mild in the middle hippocampus, inferior parietal and lateral temporal cortex and absent in other regions. NFT density was greatest in the posterior hippocampus followed by middle hippocampus, entorhinal cortex and amygdala. LB were also most numerous in limbic regions but unlike NFT, were also widespread in the neocortex (Figure 4).

Among the analyzed ROIs we identified the greatest PiB retention (PiB retention ratio >1.90), and Aβ density in the frontal lobe and medial parietal ROIs (Table). There was a strong correlation between PiB retention and Aβ density in the 17 ROIs that were analyzed on pathological examination using Spearman rank order correlation ($r=0.899$; $p<0.0001$) (Figure 5). There was no correlation between LB density and PiB retention ($r=0.13$; $p=0.66$) (Figure 6); nor between tau density and PiB retention ($r=-0.36$; $p=0.17$).

4. Discussion

The case had many of the diagnostic features of DLB; all core clinical features and presence of RBD preceding his cognitive/motor/neuropsychiatric features by decades [Boeve,2009, McKeith, et al.,2005] and a typical DLB neuropsychological pattern of impairment [Ferman, et al.,2006], with the only notable or atypical clinical finding being lack of response to any agents which often provide at least modest benefit to those with DLB. At autopsy, the patient fulfilled the criteria for neocortical LB disease with low likelihood of AD, in agreement with most of the antemortem clinical data.

Contrary to the clinical and pathological diagnosis, the pattern of FDG-PET hypometabolism suggested coexisting AD and the cortical PiB retention ratio on PET was positive (1.68) according to the generally accepted cut-off of 1.50. Diffuse plaques, on average were 2 to 3 times more abundant than the neuritic plaques on modified Bielschowsky silver stain in regions that are standard for the diagnostic evaluation for AD [Mirra, et al.,1991], and significantly contributed to the PiB retention. For example, midfrontal cortex had one of the highest PiB retention ratio (1.92), with sparse neuritic plaques. Since diffuse plaques were >3 times more common compared to the neuritic plaques in this region, we conclude that diffuse plaques significantly contributed to the PiB retention. This trend was also present in the anterior cingulate gyrus and precuneus ROIs that had some of the highest PiB retention ratios (>1.90). A similar observation was reported in two cases with Parkinson disease with dementia who were PiB positive with a high burden of diffuse plaques, but had a low likelihood of AD according to NIA-Reagan criteria at autopsy. Because of the neocortical LB pathology, dementia was attributed to the LB disease rather than diffuse plaques [Burack, et al.,2010].

The specificity of PiB binding to Aβ has been confirmed with in vitro studies [Klunk, et al., 2003]. In the human brain, PiB labels both neuritic and diffuse plaques, although labeling of diffuse/amphorous plaques is less prominent than compact/cored plaques. PiB does not label the diffuse plaques in the molecular layer of the cerebellum, which is one of the reasons for using the cerebellar PiB retention as an internal reference region for quantitative analysis [Ikonomovic, et al.,2008, Lopresti, et al.,2005]. The pathological criteria however

emphasizes neuritic plaques over the diffuse plaques for the diagnosis of AD [McKhann, et al.,1984]. Diffuse plaques are more common than neuritic plaques in DLB [Dickson,2002]. Diffuse plaques can be numerous even in cognitively normal individuals [Davis, et al.,1999, Dickson, et al.,1992, Knopman, et al.,2003]. In a patient with mild AD (clinical dementia rating = 0.5) who had low cortical PiB binding potential, diffuse plaques were the most prominent pathology observed at autopsy. It was noted that substantial densities of diffuse plaques are not benign and can be associated with early AD symptoms [Cairns, et al.,2009]. However this case also had Braak III neurofibrillary pathology, which may have contributed to the mild memory impairment.

The strong correlation between *in vivo* PiB retention and Aβ density identified in the current study is in agreement with a previous report on an AD case using a similar imaging and histology ROI matching procedure [Ikonomovic, et al.,2008]. The pathological findings however are significantly different. The case in the earlier report had advanced AD but did not have LB pathology. Whereas the predominant pathology in the current case was LB disease with low likelihood of AD pathology. Agreement between both data sets confirms the specificity of *in vivo* PiB retention, and indicates that the strong relationship between *in vivo* PiB retention and Aβ density is independent of α-synuclein LB load along the AD-DLB spectrum.

Diffuse plaques contribute significantly to PiB retention in LB diseases [Burack, et al.,2010, Dickson,2002], but the distinction between neuritic and diffuse plaques was not possible with PiB-PET in the case we studied. Increased PiB retention in a case with a low likelihood of AD emphasizes the fact that although PIB is considered as a golden standard of amyloid imaging today, the exact mechanism behind the PIB-amyloid interaction and the pathological diagnosis of AD is still not clear. Furthermore, whether diffuse plaques that contribute to PiB retention represent a preliminary stage in the pathogenesis of the neurotoxic degeneration requires further investigation [Dickson,1997, Guillozet, et al.,1997, Price, et al.,2009]. Determining the influence of **A**β on the clinical phenotype [Rowe, et al., 2007], and the relationship between diffuse plaques and cognitive impairment in DLB will be important for making treatment decisions with the availability of anti-amyloid agents.

Acknowledgments

This study was supported by the Paul B. Beeson Career Development Award in Aging K23-AG030935, P50-AG16574/Project1, P30-AG010161, RO1-AG15866, R01-AG11378, Alexander family, and the Robert H. and Clarice Smith and Abigail Van Buren Alzheimer's Disease Research Program.

References

Ashburner J, Friston KJ. Unified segmentation. Neuroimage. 2005; 26(3):839–51. [PubMed: 15955494]

Bacskai BJ, Frosch MP, Freeman SH, Raymond SB, Augustinack JC, Johnson KA, Irizarry MC, Klunk WE, Mathis CA, DeKosky ST, Greenberg SM, Hyman BT, Growdon JH. Molecular Imaging With Pittsburgh Compound B Confirmed at Autopsy: A Case Report. Arch Neurol %R 101001/archneur643431. 2007; 64(3):431–4.

Bennett DA, Schneider JA, Wilson RS, Bienias JL, Arnold SE. Neurofibrillary tangles mediate the association of amyloid load with clinical Alzheimer disease and level of cognitive function. Arch Neurol. 2004; 61(3):378–84. [PubMed: 15023815]

Boeve BF. REM sleep behavior disorder: Updated review of the core features, the REM sleep behavior disorder-neurodegenerative disease association, evolving concepts, controversies, and future directions. Ann NY Acad Sci. 2009; 1184:17–56.

Braak H, Braak E. Neuropathological stageing of Alzheimer-related changes. Acta Neuropathologica. 1991; 82(4):239–59. [PubMed: 1759558]

Burack MA, Hartlein J, Flores HP, Taylor-Reinwald L, Perlmutter JS, Cairns NJ. In vivo amyloid imaging in autopsy-confirmed Parkinson disease with dementia. Neurology. 2010; 74(1):77–84. [PubMed: 20038776]

Cairns NJ, Ikonomovic MD, Benzinger T, Storandt M, Fagan AM, Shah AR, Reinwald LT, Carter D, Felton A, Holtzman DM, Mintun MA, Klunk WE, Morris JC. Absence of Pittsburgh compound B detection of cerebral amyloid beta in a patient with clinical, cognitive, and cerebrospinal fluid markers of Alzheimer disease: a case report. Arch Neurol. 2009; 66(12):1557–62. [PubMed: 20008664]

Davis DG, Schmitt FA, Wekstein DR, Markesbery WR. Alzheimer neuropathologic alterations in aged cognitively normal subjects. J Neuropathol Exp Neurol. 1999; 58(4):376–88. [PubMed: 10218633]

Dickson DW. The pathogenesis of senile plaques. J Neuropathol Exp Neurol. 1997; 56(4):321–39. [PubMed: 9100663]

Dickson DW. Dementia with Lewy bodies: neuropathology. J Geriatr Psychiatry Neurol. 2002; 15(4): 210–6. [PubMed: 12489917]

Dickson DW, Crystal HA, Mattiace LA, Masur DM, Blau AD, Davies P, Yen SH, Aronson MK. Identification of normal and pathological aging in prospectively studied nondemented elderly humans. Neurobiol Aging. 1992; 13(1):179–89. [PubMed: 1311804]

Edison P, Rowe CC, Rinne JO, Ng S, Ahmed I, Kemppainen N, Villemagne VL, O'Keefe G, Nagren K, Chaudhury KR, Masters CL, Brooks DJ. Amyloid load in Parkinson's disease dementia and Lewy body dementia measured with [11C]PIB positron emission tomography. J Neurol Neurosurg Psychiatry. 2008; 79(12):1331–8. [PubMed: 18653550]

Ferman TJ, Smith GE, Boeve BF, Graff-Radford NR, Lucas JA, Knopman DS, Petersen RC, Ivnik RJ, Wszolek Z, Uitti R, Dickson DW. Neuropsychological differentiation of dementia with Lewy bodies from normal aging and Alzheimer's disease. Clin Neuropsychol. 2006; 20(4):623–36. [PubMed: 16980250]

Fodero-Tavoletti MT, Smith DP, McLean CA, Adlard PA, Barnham KJ, Foster LE, Leone L, Perez K, Cortes M, Culvenor JG, Li QX, Laughton KM, Rowe CC, Masters CL, Cappai R, Villemagne VL. In vitro characterization of Pittsburgh compound-B binding to Lewy bodies. J Neurosci. 2007; 27(39):10365–71. [PubMed: 17898208]

Galasko D, Hansen LA, Katzman R, Wiederholt W, Masliah E, Terry R, Hill LR, Lessin P, Thal LJ. Clinical-neuropathological correlations in Alzheimer's disease and related dementias. Arch Neurol. 1994; 51(9):888–95. [PubMed: 8080388]

Guillozet AL, Smiley JF, Mash DC, Mesulam MM. Butyrylcholinesterase in the life cycle of amyloid plaques. Ann Neurol. 1997; 42(6):909–18. [PubMed: 9403484]

Hansen L, Salmon D, Galasko D, Masliah E, Katzman R, DeTeresa R, Thal L, Pay MM, Hofstetter R, Klauber M, et al. The Lewy body variant of Alzheimer's disease: a clinical and pathologic entity. Neurology. 1990; 40(1):1–8. [PubMed: 2153271]

Ikonomovic MD, Klunk WE, Abrahamson EE, Mathis CA, Price JC, Tsopelas ND, Lopresti BJ, Ziolko S, Bi W, Paljug WR, Debnath ML, Hope CE, Isanski BA, Hamilton RL, Dekosky ST. Post-mortem correlates of in vivo PiB-PET amyloid imaging in a typical case of Alzheimer's disease. Brain. 2008

Jack CR Jr. Lowe VJ, Senjem ML, Weigand SD, Kemp BJ, Shiung MM, Knopman DS, Boeve BF, Klunk WE, Mathis CA, Petersen RC. 11C PiB and structural MRI provide complementary information in imaging of Alzheimer's disease and amnestic mild cognitive impairment. Brain. 2008; 131(Pt 3):665–80. [PubMed: 18263627]

Joachim CL, Morris JH, Selkoe DJ. Clinically diagnosed Alzheimer's disease: autopsy results in 150 cases. Ann Neurol. 1988; 24(1):50–6. [PubMed: 3415200]

Klunk WE, Wang Y, Huang GF, Debnath ML, Holt DP, Shao L, Hamilton RL, Ikonomovic MD, DeKosky ST, Mathis CA. The binding of 2-(4′-methylaminophenyl)benzothiazole to postmortem brain homogenates is dominated by the amyloid component. J Neurosci. 2003; 23(6):2086–92. [PubMed: 12657667]

Knopman DS, Parisi JE, Salviati A, Floriach-Robert M, Boeve BF, Ivnik RJ, Smith GE, Dickson DW, Johnson KA, Petersen LE, McDonald WC, Braak H, Petersen RC. Neuropathology of cognitively normal elderly. J Neuropathol Exp Neurol. 2003; 62(11):1087–95. [PubMed: 14656067]

Kokmen E, Naessens JM, Offord KP. A short test of mental status: description and preliminary results. Mayo Clin Proc. 1987; 62(4):281–8. [PubMed: 3561043]

Lopresti BJ, Klunk WE, Mathis CA, Hoge JA, Ziolko SK, Lu X, Meltzer CC, Schimmel K, Tsopelas ND, DeKosky ST, Price JC. Simplified quantification of Pittsburgh Compound B amyloid imaging PET studies: a comparative analysis. J Nucl Med. 2005; 46(12):1959–72. [PubMed: 16330558]

Lowe VJ, Kemp BJ, Jack CR Jr. Senjem M, Weigand S, Shiung M, Smith G, Knopman D, Boeve B, Mullan B, Petersen RC. Comparison of 18F-FDG and PiB PET in cognitive impairment. J Nucl Med. 2009; 50(6):878–86. [PubMed: 19443597]

Maetzler W, Liepelt I, Reimold M, Reischl G, Solbach C, Becker C, Schulte C, Leyhe T, Keller S, Melms A, Gasser T, Berg D. Cortical PIB binding in Lewy body disease is associated with Alzheimer-like characteristics. Neurobiol Dis. 2009; 34(1):107–12. [PubMed: 19162186]

Maetzler W, Reimold M, Liepelt I, Solbach C, Leyhe T, Schweitzer K, Eschweiler GW, Mittelbronn M, Gaenslen A, Uebele M, Reischl G, Gasser T, Machulla HJ, Bares R, Berg D. [11C]PIB binding in Parkinson's disease dementia. Neuroimage. 2008; 39(3):1027–33. [PubMed: 18035558]

McKeith IG, Dickson DW, Lowe J, Emre M, O'Brien JT, Feldman H, Cummings J, Duda JE, Lippa C, Perry EK, Aarsland D, Arai H, Ballard CG, Boeve B, Burn DJ, Costa D, Del Ser T, Dubois B, Galasko D, Gauthier S, Goetz CG, Gomez-Tortosa E, Halliday G, Hansen LA, Hardy J, Iwatsubo T, Kalaria RN, Kaufer D, Kenny RA, Korczyn A, Kosaka K, Lee VM, Lees A, Litvan I, Londos E, Lopez OL, Minoshima S, Mizuno Y, Molina JA, Mukaetova-Ladinska EB, Pasquier F, Perry RH, Schulz JB, Trojanowski JQ, Yamada M. Diagnosis and management of dementia with Lewy bodies: third report of the DLB Consortium. Neurology. 2005; 65(12):1863–72. [PubMed: 16237129]

McKhann G, Drachman D, Folstein M, Katzman R, Price D, Stadlan EM. Clinical diagnosis of Alzheimer's disease: report of the NINCDS-ADRDA Work Group under the auspices of Department of Health and Human Services Task Force on Alzheimer's Disease. Neurology. 1984; 34(7):939–44. [PubMed: 6610841]

Mirra SS, Heyman A, McKeel D, Sumi SM, Crain BJ, Brownlee LM, Vogel FS, Hughes JP, van Belle G, Berg L. The Consortium to Establish a Registry for Alzheimer's Disease (CERAD). Part II. Standardization of the neuropathologic assessment of Alzheimer's disease. Neurology. 1991; 41(4):479–86. [PubMed: 2011243]

Mufson EJ, Mash DC, Hersh LB. Neurofibrillary tangles in cholinergic pedunculopontine neurons in Alzheimer's disease. Ann Neurol. 1988; 24(5):623–9. [PubMed: 3202615]

Price JL, McKeel DW Jr. Buckles VD, Roe CM, Xiong C, Grundman M, Hansen LA, Petersen RC, Parisi JE, Dickson DW, Smith CD, Davis DG, Schmitt FA, Markesbery WR, Kaye J, Kurlan R, Hulette C, Kurland BF, Higdon R, Kukull W, Morris JC. Neuropathology of nondemented aging: presumptive evidence for preclinical Alzheimer disease. Neurobiol Aging. 2009; 30(7):1026–36. [PubMed: 19376612]

Rowe CC, Ng S, Ackermann U, Gong SJ, Pike K, Savage G, Cowie TF, Dickinson KL, Maruff P, Darby D, Smith C, Woodward M, Merory J, Tochon-Danguy H, O'Keefe G, Klunk WE, Mathis CA, Price JC, Masters CL, Villemagne VL. Imaging beta-amyloid burden in aging and dementia. Neurology. 2007; 68(20):1718–25. [PubMed: 17502554]

Schneider JA, Arvanitakis Z, Bang W, Bennett DA. Mixed brain pathologies account for most dementia cases in community-dwelling older persons. Neurology. 2007; 69(24):2197–204. [PubMed: 17568013]

Schneider JA, Bienias JL, Gilley DW, Kvarnberg DE, Mufson EJ, Bennett DA. Improved detection of substantia nigra pathology in Alzheimer's disease. J Histochem Cytochem. 2002; 50(1):99–106. [PubMed: 11748299]

Senjem ML, Gunter JL, Shiung MM, Petersen RC, Jack CR Jr. Comparisson of different methodological implementations of voxel-based morphometry in neurodegenerative disease. Neuroimage. 2005; 26:370–6.

Thal LJ, Kantarci K, Reiman EM, Klunk WE, Weiner MW, Zetterberg H, Galasko D, Pratico D, Griffin S, Schenk D, Siemers E. The role of biomarkers in clinical trials for Alzheimer disease. Alzheimer Dis Assoc Disord. 2006; 20(1):6–15. [PubMed: 16493230]

Zaccai J, McCracken C, Brayne C. A systematic review of prevalence and incidence studies of dementia with Lewy bodies. Age Ageing. 2005; 34(6):561–6. [PubMed: 16267179]

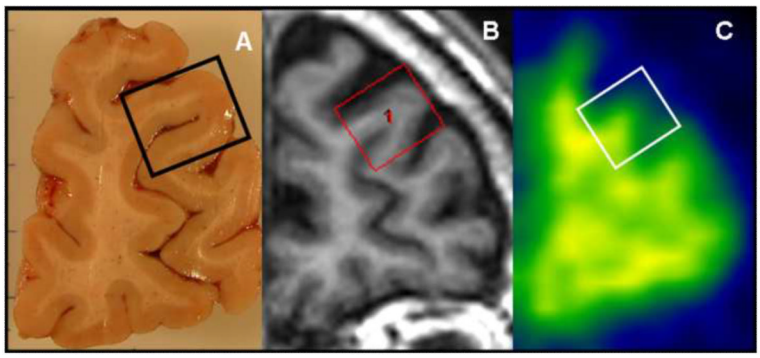

Figure 1. ROI-based analysis of the histopathological and imaging data

Tissue section from the right hemisphere and the tissue block from the rostral middle frontal gyrus are displayed (A). 3D MRI is manually reoriented for anatomical matching to the tissue section and the region of interest (ROI) simulating the tissue block is manually placed on the MRI (B). The PiB retention ratio image and the registered ROI is shown (C). Correlations were performed between PiB retention ratio from the ROI (masked with the segmented gray matter and corrected for CSF partial volume averaging) and the Aβ, Lewy body α-synuclein and PHF-tau neurofibrillary tangle densities from the tissue block.

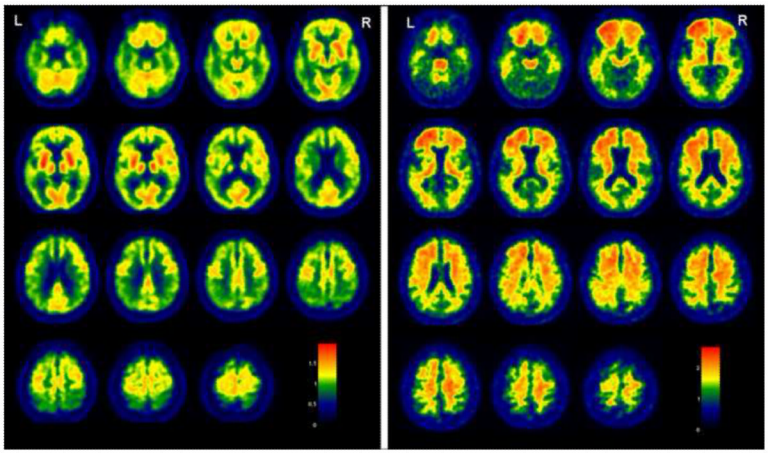

Figure 2. Representative slices from PiB-PET and FDG-PET images

Marked reduction in glucose metabolism is present in the temporal and parietal as well as the prefrontal cortex on 18F-FDG PET (left). PiB retention ratio maps are presented. Greatest PiB retention is seen in the frontal lobes, where as the occipital lobes are relatively spared (right)

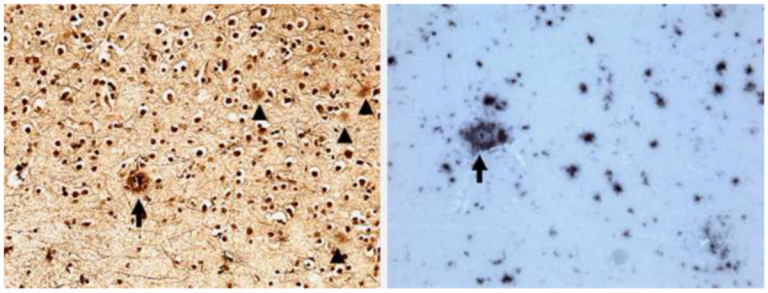

Figure 3. Aβ plaques in midfrontal cortex sections

Bielschowsky stain shows one neuritic plaque (arrow), and several diffuse plaques (arrow heads) (left); anti Aβ immunostaining in same region shows neuritic plaque (arrow) and abundant diffuse amyloid deposition (right). Original magnification 200X.

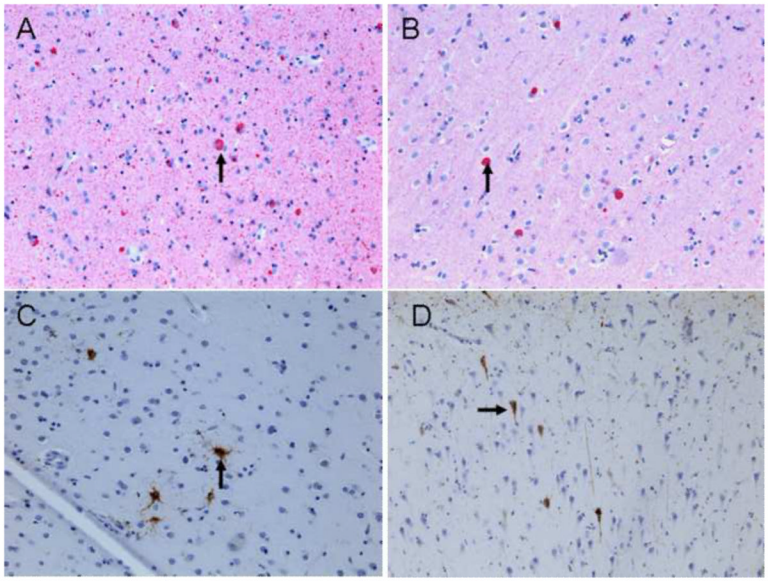

Figure 4. α-synuclein immunoreactive LBs and PHF-tau immunoreactive NFTs

Anti α-synuclein immunostaining shows LBs (arrows) throughout entorhinal cortex (A) and midfrontal cortex (B); Anti PHF-tau (AT8) immunostaining shows isolated NFTs (arrows) in the neurons of midfrontal cortex (C) and throughout the CA1 sector of hippocampus (D) (200x).

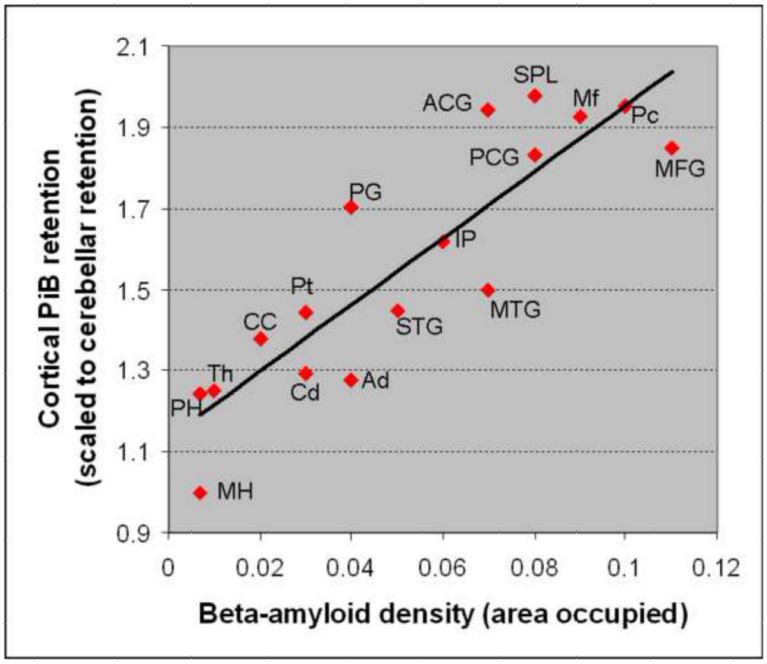

Figure 5. Correlation between Cortical PiB retention ratio and Aβ density

2 MH: middle hippocampus; PH: posterior hippocampus; Th: thalamus; Cd: caudate; Ad: amygdala; CC: calcarine cortex; Pt: putamen; STG: superior temporal gyrus; MTG: middle temporal gyrus; IP: inferior parietal; PG: precentral gyrus; PCG: posterior cingulate gyrus; MFG: middle frontal gyrus; Mf: midfrontal; ACG: anterior cingulate gyrus; Pc: Precuneus; SPL: superior parietal lobule.

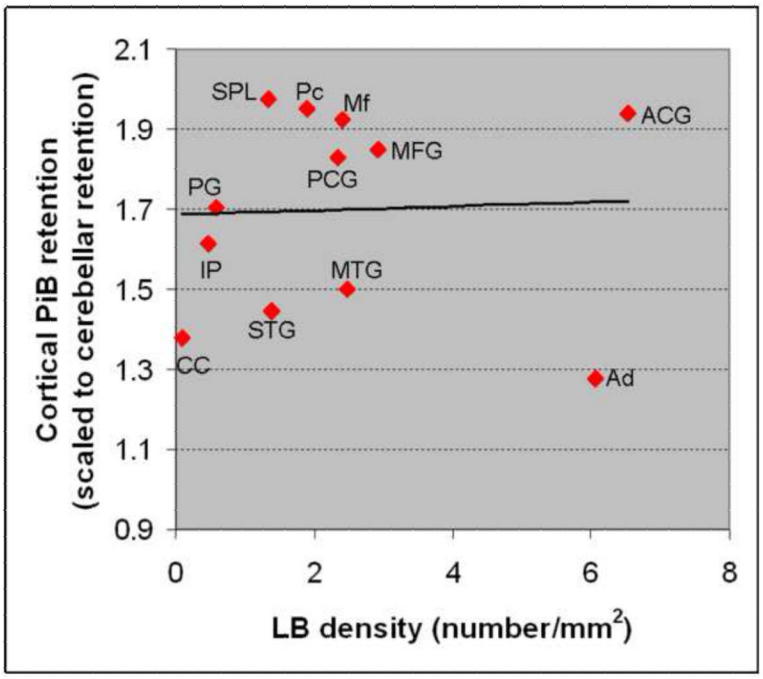

Figure 6. Correlation between Cortical PiB retention ratio and LB density

Ad: amygdala; CC: calcarine cortex; STG: superior temporal gyrus; MTG: middle temporal gyrus; IP: inferior parietal; PG: precentral gyrus; PCG: posterior cingulate gyrus; MFG: middle frontal gyrus; Mf: midfrontal; ACG: anterior cingulate gyrus; Pc: Precuneus; SPL: superior parietal lobule.

Table

PiB retention ratio and the distribution and magnitude of AD and LB pathology in different brain regions of interest*

	PiB retention ratio	Neuritic plaques**	Diffuse plaques**	Amyloid load	NFT density	LB density
Diagnostic regions						
Midfrontal	1.92	5	16	0.09	0.02	2.41
Middle temporal gyrus	1.50	5	11	0.07	0.02	2.48
Entorhinal cortex***	N/A	3	15	0.06	4.3	3.32
Middle hippocampus	1.00	0	0	0.007	13.25	N/A
Inferior parietal	1.62	4	13	0.06	0	0.46
Caudate	1.29	N/A	N/A	0.03	0	N/A
Putamen	1.44	N/A	N/A	0.03	0	N/A
Thalamus	1.24	N/A	N/A	0.01	0.03	N/A
Substantia nigra***	N/A	N/A	N/A	0.01	0	4.56
Anterior cingulate gyrus	1.94	6	22	0.07	0.03	6.53
Additional regions						
Middle frontal gyrus	1.85	11	16	0.11	0.01	2.93
Amygdala	1.28	25	6	0.04	2.4	6.06
Precentral gyrus	1.70	9	11	0.04	0	0.57
Posterior hippocampus	1.24	0	0	0.007	19.57	N/A
Superior temporal gyrus	1.45	7	10	0.05	0	1.39
Posterior cingulate gyrus	1.83	8	10	0.08	0.125	2.34
Precuneus	1.95	5	12	0.1	0	1.89
Superior parietal lobule	1.98	12	11	0.08	0.009	1.33
Calcarine cortex	1.38	3	1	0.02	0	0.08

* N/A = not applicable;

** Plaque counts correspond to CERAD as follows: 1-5 = sparse; 6-19 = moderate; ≥20 = frequent (see text for description of pathology methodology)

*** Entorhinal cortex and substantia nigra regions evaluated at autopsy were not analyzed in the PiB-PET images because the sizes of the histological blocs were less than the resolution of PET in at least one dimension which did not allow reliable assessment of these regions.